J. Appl. Cryst. (1973). **6**, 466

Sample-Curvature Error in Stress Measurement made with an X-ray Diffractometer

BY A. K. SINGH* AND C. BALASINGH

Materials Science Division, National Aeronautical Laboratory, Bangalore-17, India

(*Received* 18 *August* 1972; *accepted* 4 *June* 1973)

The effect of an arbitrary sample curvature on the centroid-shift and the broadening (variance) of a diffraction-line profile is discussed for the Seemann–Bohlin geometry of a diffractometer. The errors in stress measurement arising from the curvature of the sample surface are estimated. The shift of the centroid and, hence, the error in stress increase with increasing equatorial divergence and curvature of the sample. For example, for a cylinder of radius 10 mm, $\Delta\sigma/K$ increases from 0·075° at 1° divergence to 0·32° at 2° divergence for $\psi = 0°$, 60° and Bragg angle 70°. The analysis helps one to choose the experimental parameters to keep the errors small; in case this is not possible, the expressions derived in this paper can be used to compute the correction factors. The position on the detector arm of the receiving slit corresponding to the minimum variance is different from that given by the Seemann–Bohlin parafocusing condition. However, the line-widths for the two positions do not differ appreciably.

Introduction

The measurement of the residual stresses using a powder diffractometer requires parafocusing based on Seemann–Bohlin geometry (Cullity, 1959). The effect of the geometrical factors (Wilson, 1963) on the centroid shift for a flat sample has been recently discussed by Singh & Balasingh (1971) and Gillham (1971). Quite often, one has to measure the residual stresses on samples with curved surfaces. In this paper, expressions have been derived for the centroid shift due to the curvature of the sample surface. The errors in stress measurement arising from this curvature are discussed. Further, we have considered the effect of sample curvature on the broadening of a diffraction line. The principle of minimizing the total variance with respect to sample-to-receiving-slit distance (Singh & Balasingh, 1972) has been applied to obtain the position of the receiving slit on the detector arm. Some numerical calculations are presented for a cylindrical specimen with its axis parallel to the diffractometer axis.

Basic equations

We shall follow the method used for the analysis of flat samples (Singh & Balasingh, 1971). The notation used is defined in Appendix A. A parameter 2ε, is expressed in terms of the components of the vectors $\mathbf{x}_r$, $\mathbf{x}_s$ and $\mathbf{x}_f$ as follows:

$$\begin{aligned}(2\varepsilon) = (\eta S)^{-1}[&x_s\{\cos(\varphi-\psi)+\eta\cos(\varphi+\psi)\}\\ &+y_s\{\sin(\varphi-\psi)-\eta\sin(\varphi+\psi)\}+y_r+\eta y_f]\\ &+\tfrac{1}{2}S^{-2}y_S^2[\sin(\varphi+\psi)-\eta^{-1}\sin(\varphi-\psi)\}^2\cot 2\varphi\\ &+\{\sin 2(\varphi+\psi)+\eta^{-2}\sin 2(\varphi-\psi)\}]\\ &+S^{-2}[-x_f y_s\sin(\varphi+\psi)-\eta^{-2}x_r y_s\sin(\varphi-\psi)]\\ &+\eta^{-1}S^{-2}[z_S^2\{1+\tfrac{1}{2}(\eta+\eta^{-1})\cos 2\varphi\}\operatorname{cosec} 2\varphi\\ &+\tfrac{1}{2}z_r^2\eta^{-1}\cot 2\varphi+\tfrac{1}{2}z_f^2\eta\cot 2\varphi\\ &-z_r z_s\{1+\eta^{-1}\cos 2\varphi\}\operatorname{cosec} 2\varphi\\ &+z_r z_f\operatorname{cosec} 2\varphi-z_f z_s\{1+\eta\cos 2\varphi\}\operatorname{cosec} 2\varphi]\,. \quad (1)\end{aligned}$$

The centroid shift due to the various terms in equation (1) can be obtained by taking their averages. To a good approximation, the axial terms (*i.e.* terms containing z components) are not affected by the sample curvature, and therefore, the expressions for the centroid shift derived by Singh & Balasingh (1971) are valid in the present case also. The sample curvature leads to a displacement of the sample surface from the focusing circle. The centroid shift arising from this can be derived by taking an average of the terms in x_s (see also Appendix *B*). The terms in y_s are slightly affected by the sample curvature because of the slight dependence of A_1 and A_2 on sample curvature.

Sample-curvature error

A line focus is often used in powder diffractometry and the axial divergence is limited by Soller slits. A cylindrical sample with a radius R_F and its axis parallel to the diffractometer axis, will be required to focus the diffracted beam in the equatorial plane. Let us consider a specimen surface having an arbitrary curvature and let x_S be represented by

$$x_S = f(y_S, z_S) \quad (2)$$

and x_F by,

$$x_F = g(y_F)\,. \quad (3)$$

At a given y and z, the displacement of the sample from its ideal position is given by,

$$\begin{aligned}x &= x_S - x_F\\ &= f(y,z) - g(y)\,. \quad (4)\end{aligned}$$

The centroid shift due to sample curvature is given by

$$\langle 2\varepsilon\rangle = (\eta S)^{-1}\{\cos(\varphi-\psi)+\eta\cos(\varphi+\psi)\}\langle x\rangle \quad (5)$$

and the variance by,

$$W = \langle(2\varepsilon)^2\rangle - \langle(2\varepsilon)\rangle^2. \quad (6)$$

It may be noted that equations (5) and (6) include the effect of the equatorial divergence, and the terms in y_S^2 need not be considered separately.

* Present address: Institute of Geophysics and Planetary Physics, University of California, Los Angeles, California 90024.

Representation of a curved surface

The evaluation of equations (5) and (6) requires equations (2) and (3) in explicit forms. We shall assume that a curved surface over a small region can be approximated to a surface generated by rotating a circular arc about a line in the plane of the arc. The resulting surface possesses two radii of curvature R_1 and R_2 and can be described by the following equation (Eisenhart, 1939):

$$4(R_2-R_1)^2\{(x_S-R_2)^2+z_S^2\} = \{2R_2(R_2-R_1)-2x_SR_2+x_S^2+y_S^2+z_S^2\}^2. \quad (7)$$

In practice, R_1 and R_2 are large compared with x_S, y_S, and z_S and equation (7) can be approximated to the following form,

$$x_S=\frac{y_S^2}{2R_1}+\frac{z_S^2}{2R_2}+\frac{y_S^4}{8R_1^3}+\frac{z_S^4}{8R_2^3}+\frac{y_S^2z_S^2}{4R_1R_2^2}. \quad (8)$$

In order to estimate the error in x_S due to the approximations in equation (8), an extreme case of a cylindrical sample with $R_1=10$ mm and a divergence of 4° is considered. The x_S values calculated from equations (7) and (8) differ by only 4%. In practice, both the curvature of the sample and the divergence of the beam are smaller than these values. Equation (8) is therefore, a good approximation of equation (7) near the origin of coordinates.

Further, it can be shown that,

$$x_F=\frac{y_F^2}{2R_F}+\frac{y_F^4}{8R_F^3}. \quad (9)$$

Centroid shift and variance

From equations (4), (8) and (9), the following expression is obtained for the centroid shift:

$$\langle 2\varepsilon\rangle=(\eta S)^{-1}\{\cos(\varphi-\psi)+\eta\cos(\varphi+\psi)\} \times\left\{\tfrac{1}{6}\left(\frac{1}{R_1}-\frac{1}{R_F}\right)X(3)+\tfrac{1}{6}\frac{P^2}{R_2}+\tfrac{1}{40}\left(\frac{1}{R_1^3}-\frac{1}{R_F^3}\right) \times X(5)+\tfrac{1}{40}\frac{P^4}{R_2^3}+\tfrac{1}{36}\frac{P^2}{R_1R_2^2}X(3)\right\}. \quad (10)$$

The expression for the variance is given by,

$$W=(\eta S)^{-2}[\cos(\varphi-\psi)+\eta\cos(\varphi+\psi)]^2 \times\left[\left(\frac{1}{R_1}-\frac{1}{R_F}\right)^2\{\tfrac{1}{20}X(5)-\tfrac{1}{36}X^2(3)\}+\tfrac{1}{45}\frac{P^4}{R_2^2} +\left(\frac{1}{R_1}-\frac{1}{R_F}\right)\left(\frac{1}{R_1^3}-\frac{1}{R_F^3}\right)\{\tfrac{1}{56}X(7)-\tfrac{1}{120}X(3)X(5)\} +\tfrac{1}{105}\frac{P^6}{R_2^4}+\left(\frac{1}{R_1^3}-\frac{1}{R_F^3}\right)^2\{\tfrac{1}{572}X(9)-\tfrac{1}{1000}X^2(5)\} +\tfrac{1}{900}\frac{P^8}{R_2^6}+\tfrac{1}{630}\frac{P^6}{R_1R_2^5}X(3)+\frac{P^4}{R_1^2R_2^4}\{\tfrac{1}{400}X(5) -\tfrac{1}{1296}X^2(3)\}+\tfrac{1}{135}\frac{P^4}{R_1R_2^3}X(3) +\frac{P^2}{R_1R_2^2}\left(\frac{1}{R_1}-\frac{1}{R_F}\right)\{\tfrac{1}{60}X(5)-\tfrac{1}{108}X^2(3)\} +\frac{P^2}{R_1R_2^2}\left(\frac{1}{R_1^3}-\frac{1}{R_F^3}\right)\{\tfrac{1}{336}X(7)-\tfrac{1}{720}X(5)X(3)\}\right]. \quad (11)$$

When the numerical values of $\langle 2\varepsilon\rangle$ and W are calculated, φ on the right-hand side of equations (10) and (11) can be replaced by θ without the introduction of any appreciable error.

Error in stress measurement

In practice, the two exposure method with $\psi=0°$, 45° or $\psi=0°$, 60° is used for stress measurement. The error introduced in stresses by the curvature of the sample is given by

$$\Delta\sigma=K[\langle 2\varepsilon\rangle_{\psi=45°\ (60°)}-\langle 2\varepsilon\rangle_{\psi=0}]. \quad (12)$$

$\langle 2\varepsilon\rangle_\psi$ is given by equation (10). $\Delta\sigma$ should be subtracted from the measured value of σ to obtain the correct value. For a numerical estimate of this error, it is more convenient to consider $\Delta\sigma/K$ instead of $\Delta\sigma$. In the next section, the numerical values of $\Delta\sigma/K$ for cylindrical samples are estimated.

Cylindrical sample

A cylindrical sample with its axis parallel to the diffractometer axis (shown in Fig. 1) is often used. Hence, we shall discuss in detail the centroid shift for a cylindrical sample. The expression for the centroid shift for a cylindrical sample can be obtained by substituting $R_2=\infty$ in equation (10). This gives,

$$\langle 2\varepsilon\rangle_{\text{Cyl.}}=(\eta S)^{-1}\{\cos(\varphi-\psi)+\eta\cos(\varphi+\psi)\} \times\left\{\tfrac{1}{6}\left(\frac{1}{R_1}-\frac{1}{R_F}\right)X(3)+\tfrac{1}{40}\left(\frac{1}{R_1^3}-\frac{1}{R_F^3}\right)X(5)\right\}. \quad (13)$$

$\langle 2\varepsilon\rangle$ *vs.* ψ plots for $R_1=10$ mm and various values of θ and 2α are given in Fig. 2. For a given value of θ and ψ, $\langle 2\varepsilon\rangle$ decreases with decreasing values of divergence.

In order to estimate the errors introduced in stress measurements on cylindrical samples, $\Delta\sigma/K$ *vs.* θ plots are shown in Figs. 3–6. It is seen from these Figures that for given R_1 and θ values, $\Delta\sigma/K$ can be made small by choosing a small value of equatorial divergence; for example, the parameters chosen in Fig. 3 lead to small errors. In practice, the divergence cannot be reduced below a certain value as it leads to a drop in the intensity. For large divergences the errors may be large; the parameters chosen for Figs. 4–6 lead to appreciable errors. For the two-exposure method with $\psi=0°$, 60°, which is often used to improve the sensitivity of the

measurement, the errors are larger than the $\psi = 0°, 45°$ setting under identical conditions.

Broadening due to curvature

The position on the detector arm of the receiving slit is determined in these experiments, by the condition,

$$R = S\frac{\sin(\theta-\psi)}{\sin(\theta+\psi)}$$

$$\frac{R}{S} = \eta_F = \frac{\sin(\theta-\psi)}{\sin(\theta+\psi)}, \qquad (14)$$

which is valid for a sample with radius of curvature R_F. An arbitrary curvature of the sample will lead to certain amount of broadening. It is of interest to determine whether equation (14) still gives the position of best focus. For this purpose, we take variance as a measure of the width of a diffraction line and express the total variance due to the geometrical factors as a function of R. The value of R corresponding to the minimum variance gives the position of best focus. This approach for investigating the effect of geometrical factors on the position of the receiving slit was first suggested by the authors (Singh & Balasingh, 1972). As discussed in the above reference, the variances due to all the terms in equation (1), except that due to the y_s term, vary rather slowly with η. In the present discussion therefore, only the variances due to the sample curvature and the y_s term are considered. Further, the discussions are confined to cylindrical samples with their axes parallel to the diffractometer axis. The variance due to the curvature of a cylindrical sample can be obtained by letting $R_2 = \infty$ in equation (11), which then reduces to,

$$W_1 = (\eta S)^{-2}\{\cos(\varphi-\psi)+\eta\cos(\varphi+\psi)\}^2 \times \left[\left(\frac{1}{R_1}-\frac{1}{R_F}\right)^2\{\tfrac{1}{20}X(5)-\tfrac{1}{36}X^2(3)\} + \left(\frac{1}{R_1}-\frac{1}{R_F}\right)\left(\frac{1}{R_1^3}-\frac{1}{R_F^3}\right)\{\tfrac{1}{56}X(7)-\tfrac{1}{120}X(3)X(5)\} + \left(\frac{1}{R_1^3}-\frac{1}{R_F^3}\right)^2\{\tfrac{1}{576}X(9)-\tfrac{1}{1600}X^2(5)\}\right], \qquad (15)$$

and the variance due to the y_s term is given by,

$$W_2 = (\eta S)^{-2}\{\sin(\varphi-\psi)-\eta\sin(\varphi+\psi)\}^2 \times\{\tfrac{1}{3}(A_2^2-A_1A_2+A_1^2)-\tfrac{1}{4}(A_2-A_1)\}. \qquad (16)$$

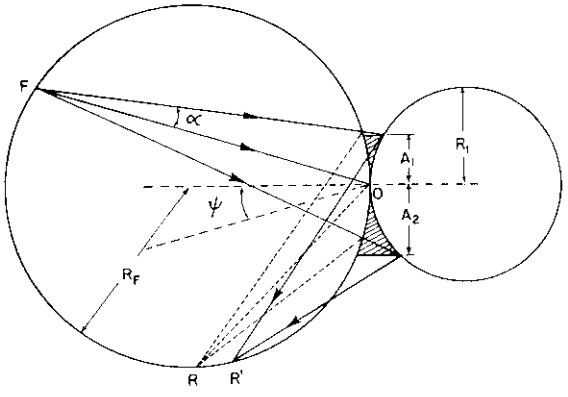

Fig. 1. The ray diagram in the equatorial plane showing the focusing circle of radius R_F and a sample of radius R_1.

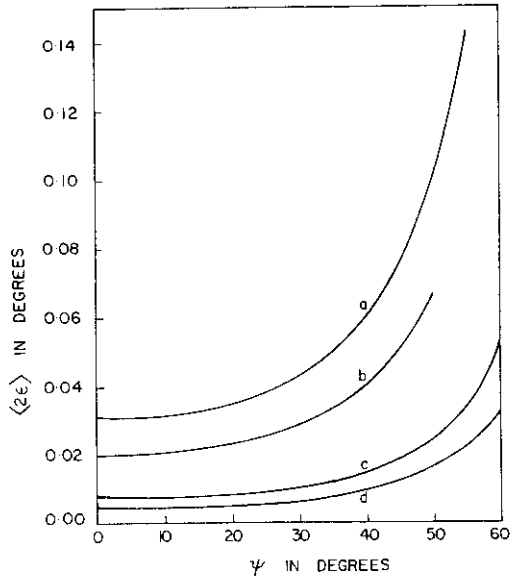

Fig. 2. Plot of $\langle 2\varepsilon\rangle_{cyl}$ *vs.* ψ. $R_1 = 10$ mm and $S = 170$ mm. (*a*) $\theta = 75°$ and $2\alpha = 2°$, (*b*) $\theta = 80°$ and $2\alpha = 2°$, (*c*) $\theta = 75°$ and $2\alpha = 1°$, (*d*) $\theta = 80°$ and $2\alpha = 1°$. The curves (*a*) and (*b*) are terminated at $\psi = 55°$ and 50° respectively, beyond which the entire beam is not intercepted by the sample.

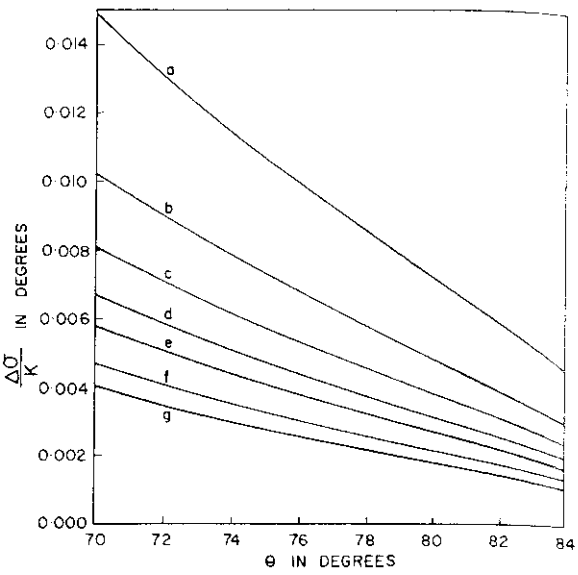

Fig. 3. Plot of $\Delta\sigma/K$ *vs.* θ for $\psi = 0°$, 45° setting and $2\alpha = 2°$. The curves (*a*) through (*g*) refer to $R_1 = 10$, 15, 20, 25, 30, 40 and 50 mm respectively.

The minimum of (W_1+W_2) with respect to η can be obtained by the condition,

$$\partial(W_1+W_2)/\partial\eta=0\,. \qquad (17)$$

The left-hand side of equation (17) is complicated; the minimum of (W_1+W_2) can be obtained numerically. As an example, (W_1+W_2) as a function of η is plotted in Fig. 7 for $\theta=75°$, $\psi=45°$, $2\alpha=3°$ and $R_1=10$ mm. The minimum variance is obtained at $\eta=0{\cdot}60$ while equation (14) gives $\eta=0{\cdot}5775$. This change in η amounts to about 4 mm change in R for a diffractometer with $S=170$ mm. The change in the position of focus is therefore, appreciable. A plot of $\eta(W_{\min})/\eta_F$ as a function of θ is shown in Fig. 8 for a few values of R_1. It is seen that this ratio departs from unity appreciably only for large 2α and small R_1. However, the advantage gained in terms of of the decrease in the width of the line is not appreciable, especially if we consider the variances due to the other terms also.

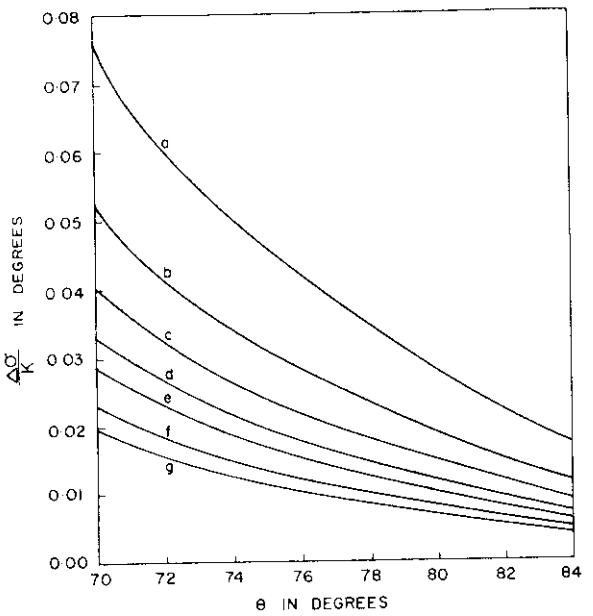

Fig. 4. Plot of $\Delta\sigma/K$ *vs.* θ for $\psi=0°$, 60° setting and $2\alpha=1°$. The curves (a) through (g) refer to $R_1=10$, 15, 20, 25, 30, 40 and 50 mm respectively.

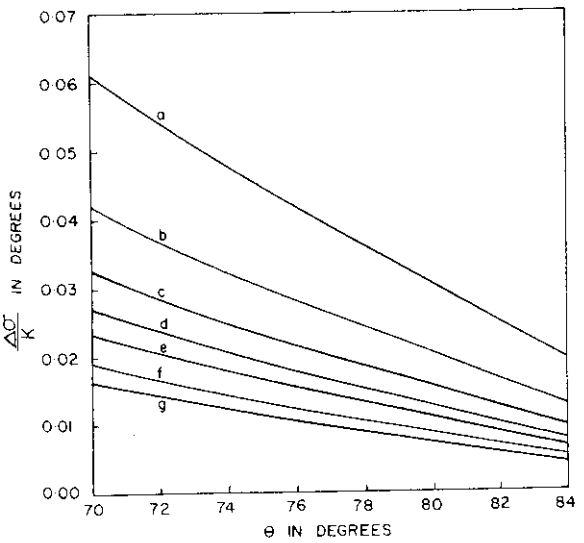

Fig. 5. Plot of $\Delta\sigma/K$ *vs.* θ for $\psi=0°$, 45° setting and $2\alpha=2°$. The curves (a) through (g) refer to $R_1=10$, 15, 20, 25, 30, 40 and 50 mm respectively.

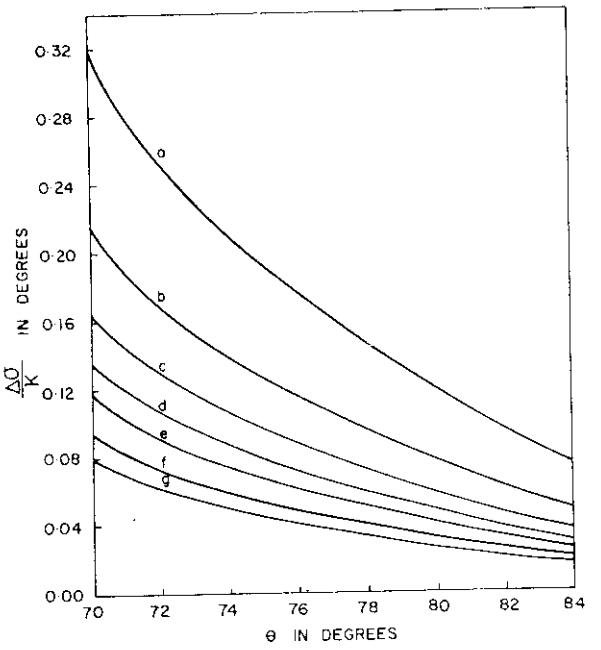

Fig. 6. Plot of $\Delta\sigma/K$ *vs.* θ for $\psi=0°$, 60° setting and $2\alpha=2°$. The curves (a) through (g) refer to $R_1=10$, 15, 20, 25, 30, 40 and 50 mm respectively.

Conclusion

The expressions deduced in this paper enable us to estimate the centroid shift due to the sample curvature and the resulting errors in the measurement of stresses. The analysis may serve as an useful guideline in choosing 2α to keep the errors in stresses below a desired value. If 2α cannot be reduced below a certain value, because it leads to a considerable drop in intensity, the errors can be estimated. The curvature of the sample leads to appreciable broadening which is determined jointly by the sample-curvature and 2α. The position of the minimum variance is appreciably different from that obtained from the Seemann–Bohlin parafocusing condition. However, the variance does not vary markedly with R, and therefore, placing the slit at the position of minimum variance does not reduce the width significantly.

The authors wish to thank Dr S. Ramaseshan for his keen interest in the work.

APPENDIX A

Notation

R – distance between the receiving slit and the diffractometer axis.
S – distance between the source and the diffractometer axis.
η – equal to R/S.
θ – Bragg angle.
φ – position of the detector arm.
ε – equal to $(\theta-\varphi)$.
$\mathbf{x}_r$ – a vector defining a point in the receiving slit.
x_r, y_r, z_r – components of $\mathbf{x}_r$, respectively parallel to **R**, perpendicular to **R** and parallel to the diffractometer axis.
$\mathbf{x}_f$ – a vector defining a point in the focal spot.
x_f, y_f, z_f – component of $\mathbf{x}_f$, respectively parallel to **S**, perpendicular to **S** and parallel to the diffractometer axis.
$\mathbf{x}_s$ – a vector defining a point in the specimen.
x_s, y_s, z_s – components of $\mathbf{x}_s$, respectively perpendicular to the specimen surface, parallel to the specimen surface and parallel to the diffractometer axis.
ψ – angle between the reflecting plane normal and the specimen surface normal.
A_1, A_2 – maximum values of $-y_s$ and $+y_s$ respectively

$$A_1 \simeq (S\alpha)\{1-\alpha\cot(\theta+\psi) - (S\alpha/2R_1)\cos(\theta+\psi)\}/\sin(\theta+\psi)$$

$$A_2 \simeq (S\alpha)\{1+\alpha\cot(\theta+\psi) + (S\alpha/2R_1)\cos(\theta+\psi)\}/\sin(\theta+\psi)\,.$$

η_F – $\sin(\theta-\psi)/\sin(\theta+\psi)$.
R_F – radius of the focusing circle and equals $S/2\sin(\theta-\psi)$.
W – variance.
W_1 – variance due to sample curvature.
W_2 – variance due to y_s term.
R_1 – radius of curvature in equatorial plane of sample.
R_2 – radius of curvature of the sample in a plane containing the diffractometer axis and the surface normal.
$X(n)$ – equal to $(A_1^n + A_2^n)/(A_1 + A_2)$.
$2P$ – axial dimension of the illuminated area of the sample.
K – stress factor.
2α – equatorial divergence.
x_S, y_S, z_S – Cartesian coordinates of a point on the surface of the sample.
x_F, y_F – Cartesian coordinates of a point on the surface of a cylinder of radius R_F and coincident in the equatorial plane with the focusing circle.
$t(x_S, y_S)$ – path length in the sample covered by a ray incident at a point (x_S, y_S) and the ray diffracted at (x_S, y_S).
μ – linear absorption co-efficient.
σ – stress.
$\Delta\sigma$ – error in stress.

APPENDIX B

The effect of specimen transparency is to cause a centroid shift given by,

$$\langle 2\varepsilon\rangle = (\eta S)^{-1}\{\cos(\varphi-\psi)+\eta\cos(\varphi+\psi)\}\langle x_s\rangle\,.$$

where,

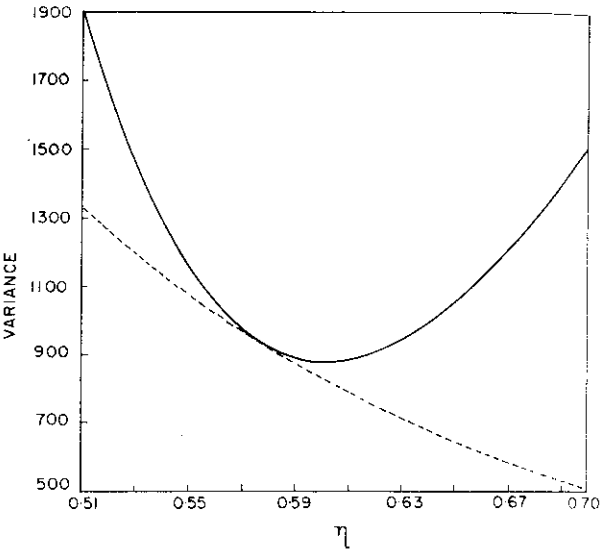

Fig. 7. (W_1+W_2) *vs.* η with $\theta=75°$, $\psi=45°$, $2\alpha=3°$ and $R_1=10$ mm. The dotted line shows the plot of W_1 *vs.* η.

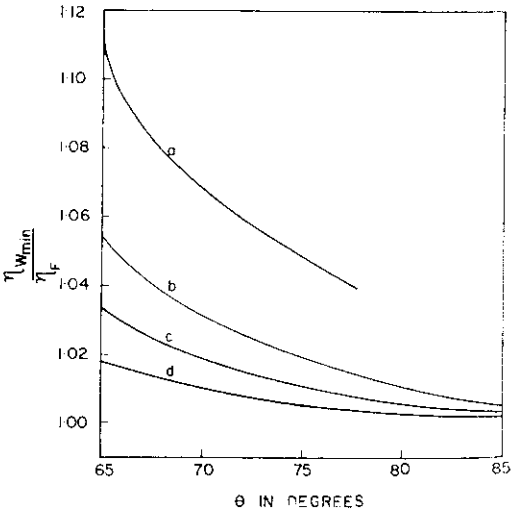

Fig. 8. Plot of $\eta(W_{min})/\eta_F$ *vs.* θ for $2\alpha=3°$ and $\psi=45°$. The curve for $R_1=10$ mm is terminated at about $\theta=78°$ beyond which the entire beam is not intercepted by the sample.

$$\langle x_s \rangle = \int_{xs}\int_{ys} x_s \exp -\mu t(x_s,y_s)\mathrm{d}x_s\mathrm{d}y_s / \times \int_{xs}\int_{ys} \exp -\mu t(x_s,y_s)\mathrm{d}x_s\mathrm{d}y_s .$$

The integral is complicated for specimens with arbitrary curvature. The values of $t(x_s,y_s)$ and $\langle x_s \rangle$ can at best, be calculated numerically. However, for samples with not too large curvatures and large μ, as is often the case in practice, the centroid shift due to specimen transparency does not deviate much from its value for flat sample (Singh & Balasingh, 1971).

References

CULLITY, B. D. (1959). *Elements of X-ray Diffraction*, pp. 444–447. New York: Addison-Wesley.

EISENHART, L. P. (1939). *Coordinate Geometry*, pp. 239–241. New York: Dover.

GILLHAM, C. J. (1971). *J. Appl. Cryst.* **4**, 498–506.

SINGH, A. K. & BALASINGH, C. (1971). *J. Appl. Phys.* **42**, 5254–5260.

SINGH, A. K. & BALASINGH, C. (1972). *J. Appl. Cryst.* **5**, 138–140.

WILSON, A. J. C. (1963). *Mathematical Theory of Powder Diffractometry*, pp. 1–45. Eindhoven: Centrex.

J. Appl. Cryst. (1973). **6**, 471

Lattice Expansions of Two Boron Carbides Between 12 and 940° C*

BY HARRY L. YAKEL

Metals and Ceramics Division, Oak Ridge National Laboratory, Oak Ridge, Tennessee 37830, *U.S.A.*

(*Received* 23 *April* 1973; *accepted* 20 *July* 1973)

High-temperature X-ray diffraction methods have been used to determine unit-cell parameters of two boron carbide compositions from 12° to about 940°C. One composition was at the carbon-rich end of the phase field (*i.e.* B_4C), the second at the boron-rich end (5 at.% C by chemical analysis). The lattice expansion of both substances was isotropic in the temperature range studied. The mean linear thermal expansion coefficient for the carbon-rich composition is $5{\cdot}65\times10^{-6}$°C^{-1}, while that of the boron-rich composition is $5{\cdot}87\times10^{-6}$°C^{-1}.

While the bulk linear thermal expansion of boron carbide† has been reported several times (Ridgway, 1934; Engberg & Zehms, 1958; Krikorian, 1960; Hedge, Kostenko & Lang, 1963), the thermal expansion coefficients of its rhombohedral (or hexagonal) unit-cell parameters have not been measured. It is of some interest to know the latter since the anisotropy of the trigonal structure of boron carbide – equal numbers of twelve-atom icosahedra and three-atom linear chains in a rock-salt structure compressed along a [111] direction (Clark & Hoard, 1943) – could give rise to anisotropy in the lattice expansion. Measurements of lattice expansions for more than one composition within the wide homogeneity range proposed for the boron carbide phase (Elliott, 1961) might also be correlated with possible structural models of the 'non-stoichiometric' material.

This paper presents results of determinations of unit-cell parameters of two boron carbide compositions at temperatures from 12° to about 940°C. One composition was at the carbon-rich end of the phase field (*i.e.*), the second at the boron-rich end. The carbon-rich material was purchased from the Norton Company, Worcester, Mass., while the boron-rich phase was prepared at this laboratory by J. P. DeLuca. Chemical analyses of the former gave the expected 20 at.% C; analyses of the latter gave only 5 at.% C, or about 4–5 at.% less than the usually accepted low-carbon limit for the phase (Elliott, 1961). Well-exposed room-temperature X-ray powder diffraction patterns of the boron-rich material showed only reflections from a boron carbide-type phase, with no indication of any reflections from a crystalline form of elemental boron. Similar patterns of the carbon-rich phase showed a minor (<5%) amount of excess graphite in addition to the dominant boron carbide.

High-temperature diffraction data were recorded in a Unicam S. 150 camera using unfiltered Cr $K\alpha$ ($\bar{\lambda}=2{\cdot}29092$ Å) radiation. Diffraction specimens consisted of powders in 0·5 mm o.d. thin-walled quartz capillaries. Temperatures were measured by a Pt, Pt–10% Rh thermocouple placed close to, but not in contact with, the diffraction specimen. Apparent thermocouple temperatures were corrected by calibration against the known lattice expansion of silver (Hume-Rothery & Reynolds, 1938). This procedure gives rise to a significant source of error in the experiment; one may not presume to know the actual specimen temperature to better than ±4°C.

Research sponsored by the U.S. Atomic Energy Commission under contract with the Union Carbide Corporation.

† One assumes that the materials studied have had the B_4C composition, though the reports are often casual in fixing the boron carbon content.